Available online at www.sciencedirect.com
SCIENCE DIRECT®
International Journal of Multiphase Flow 31 (2005) 1116–1133
International Journal of Multiphase Flow
www.elsevier.com/locate/ijmulflow

Performance characteristics of a gas–liquid–solid airlift pump

Hitoshi Fujimoto *, Takuya Nagatani, Hirohiko Takuda

Graduate School of Energy Science, Kyoto University, Kyoto 606-8501, Japan

Received 21 November 2004; received in revised form 19 June 2005

Abstract

Pump performance of a small airlift system for transporting solid particles is investigated experimentally. Six types of uprisers locally containing S-shaped portions are used to investigate the effect of local bends on the flow characteristics. The internal diameter of the upriser is 18 mm and its total height 3200 mm. Alumina particles of 3 mm diameter are used as solid particles. The relation between the discharged liquid flux and the flux of injected air are obtained, varying injected gas flux, particle flux, type of upriser, and submergence ratio. In addition, the particle motion in the upriser is investigated in detail by means of photographic observations. The physics of the phenomena is discussed from a practical viewpoint.

Keywords: Airlift pump; Gas–liquid-dispersed solid particles three-phase flow; Performance curve; Photographic observation; Non-straight uprisers

1. Introduction

The flows of liquid–air–solid particles three-phase mixtures arise in airlift systems transporting slurries or relatively large solid particles (Kato et al., 1975; Weber and Dedegil, 1976; Yoshinaga and Sato, 1996; Hatta et al., 1999; Fujimoto et al., 2003). Fig. 1 displays a schematic of an airlift system, which consists of a riser pipe and a gas injector. The liquid and dispersed solid particles

* Corresponding author. Tel.: +81 75 753 5419; fax: +81 75 753 5428.
E-mail address: h-fujimoto@energy.kyoto-u.ac.jp (H. Fujimoto).

0301-9322/$ - see front matter © 2005 Elsevier Ltd. All rights reserved.
doi:10.1016/j.ijmultiphaseflow.2005.06.008

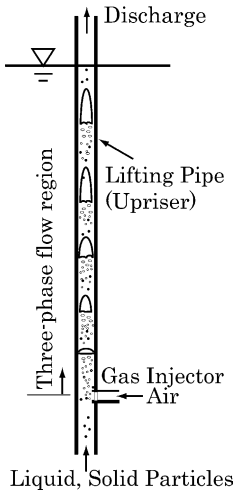

Fig. 1. Schematic of airlift pump for transporting solid particles.

flow into the upriser at the bottom end and the gas is injected at a certain point away from the bottom end. The liquid–solid particles two-phase mixture flows below the gas injector, while the three-phase flows are seen above it. The liquid and solid particles are transported vertically upward to the top end of the upriser pipe by drag and the buoyancy force of air. The pump performance, associated with the flow rate of discharged liquid as well as dispersed solid particles, is strongly dependent on the amount of air injected into the upriser.

The present authors have studied the performance of airlift pumps for transportation of solid particles experimentally as well as numerically. Hatta et al. (1999) proposed a model for predicting the efficiency of airlift pumps based on one-dimensional multi-fluid model. The predictions were compared with the experiments by other researchers for validation. Fujimoto et al. (2003) investigated the pump performance of a small airlift pump experimentally. The supplied gas flux, gas injection point, particle size, and material density of particles were systematically changed as parameters. Also, the critical boundary at which the solid particles can be lifted along the pipe was studied.

In these studies, vertically straight pipes were adopted as uprisers (see Fig. 1). It is noted that the utilization of vertically straight pipes were common in many prior works concerning airlift pumps for transportation of solid particles. This is probably to optimize operating conditions of the pump system. Since the pump efficiency of the airlift system is relatively small compared to mechanical pumps, finding the optimal operating condition is of great interest in designing such a pump system. If uprisers have local pipe bends or curved portions, loss of liquid momentum occurs in such parts, resulting in the reduction of pump performance. On the other hand, the utilization of the locally bent/curved pipes is inevitable in actual use. Extensive research using non-straight uprisers is essential from the practical viewpoint. However, few experiments have been carried out. The effect of non-straight uprisers on pump performance remains unclear.

From this standpoint, Fujimoto et al. (2004) carried out experiments using a small airlift pump containing a locally S-shaped pipe portion. The effects of the S-shaped pipe portion on the pump performance were examined using one type of S-shaped pipe. Its dimensions are shown in Fig. 2

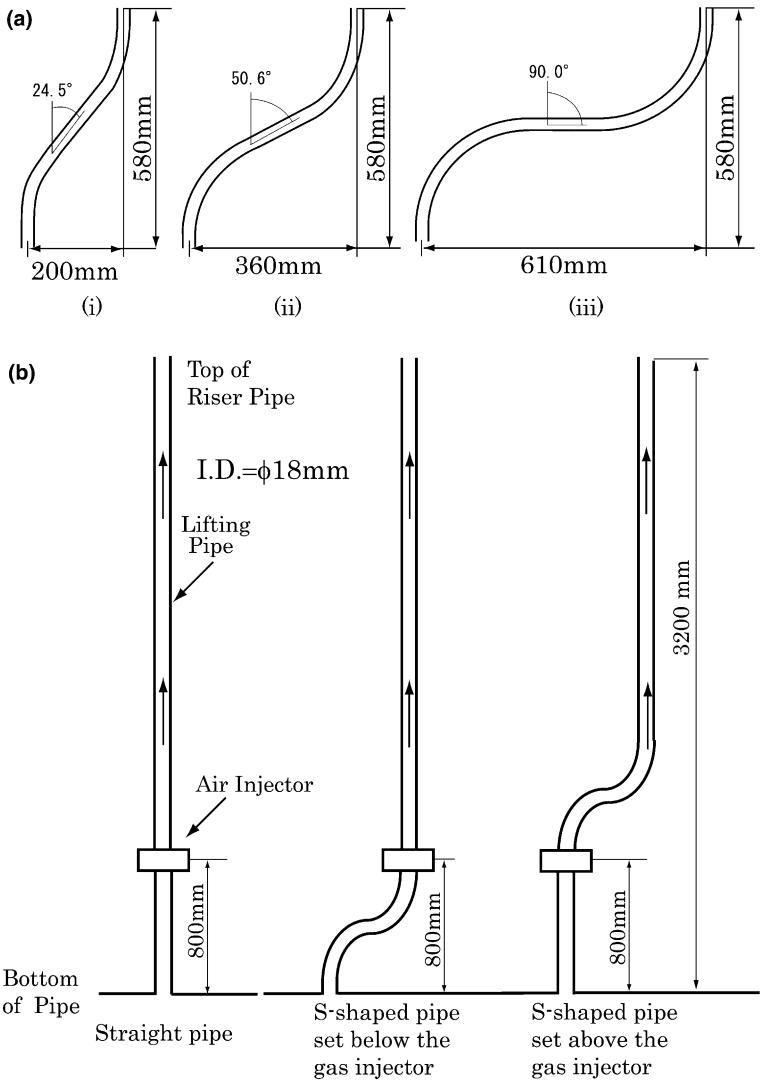

Fig. 2. (a) Dimensions of three types of S-shaped pipe and (b) three types of uprisers used in the present experiments.

as pipe (iii). It was found that reduction of pump performance occurred due to the presence of pipe bends. Also, it was observed that particle beds are formed in the horizontal portion of the S-shaped pipe attached below the gas injector. Though such interesting knowledge was obtained, more systematic experiments are essential to explore the flow characteristics in the airlift system using various types of non-straight uprisers.

In the present study, the performance of a small airlift pump in transporting solid particles was investigated. The uprisers have a local S-shaped portion above or below the gas injector. The objective of this study is to investigate the flow characteristics in the S-shaped portion. In so doing, three types of S-shaped pipes were used as shown in Fig. 2. The inclination angles in the S-shaped portion are 24.5°, 50.6°, and 90°. Tap water was used as the test liquid and alumina

particles of 3 mm diameter as solid particles. The pump performance is assessed under various experimental conditions, varying the type of pipe, the amount of injected air, and the amount of supplied particles. Also, the motion of solid particles flowing in the inclined pipe is investigated by conventional photographic observations. The transport phenomena of these multi-phase mixtures are discussed in detail.

2. Experiments

2.1. Experimental apparatus

Fig. 2(a) depicts the dimensions of S-shaped pipes used in the present study, all made of transparent glass. The inner diameter of each S-shaped pipe is 18 mm. The inclination angles of the pipes are 24.5° (i), 50.6° (ii), and 90° (iii), respectively, to the vertical line. The vertical distance between the top and bottom ends of each S-shaped pipe is fixed to 580 mm. The horizontal distance between the two ends is (i) 200 mm, (ii) 360 mm, and (iii) 610 mm, respectively. Each S-shaped pipe was set above or below the gas injector as shown in Fig. 2(b). Namely, six types of uprisers containing local bends were adopted. A straight upriser was also used for comparison. For convenience, the seven types of uprisers are called A, B, C, D, E, F, and V as shown in Table 1. The dimensions of pipe (iii) are the same used in our previous study (Fujimoto et al. (2004)).

Fig. 3 depicts the schematic of the experimental apparatus. The experimental equipment and procedures are briefly explained since they are almost the same as in our prior studies (Fujimoto et al. (2003, 2004)). The body of the airlift pump consists of a lifting pipe, a water reservoir, a suction box, a gas injector, a particle feeder, and an air separator. Spherical solid particles made of alumina with a density of $\rho_s = 3600\ \mathrm{kg/m^3}$ are 3 mm in diameter. The total height, L, of the lifting pipe is 3200 mm and the pipe diameter, d, 18 mm. The gas injector is set at $L_g = 800$ mm above the bottom end of the lifting pipe. The vertical distance, L_S, between the water level in the reservoir and the bottom of the lifting pipe can be varied. The submergence ratio, γ, is defined by the following equation:

$$\gamma = \frac{L_S - L_g}{L - L_g}. \tag{1}$$

Table 1
Types of uprisers used in the present experiments

Pipe	
A	S-shaped pipe (i) (24.5°) attached below the gas injector
B	S-shaped pipe (i) (24.5°) attached above the gas injector
C	S-shaped pipe (ii) (50.6°) attached below the gas injector
D	S-shaped pipe (ii) (50.6°) attached above the gas injector
E	S-shaped pipe (iii) (90°) attached below the gas injector
F	S-shaped pipe (iii) (90°) attached above the gas injector
V	Straight pipe

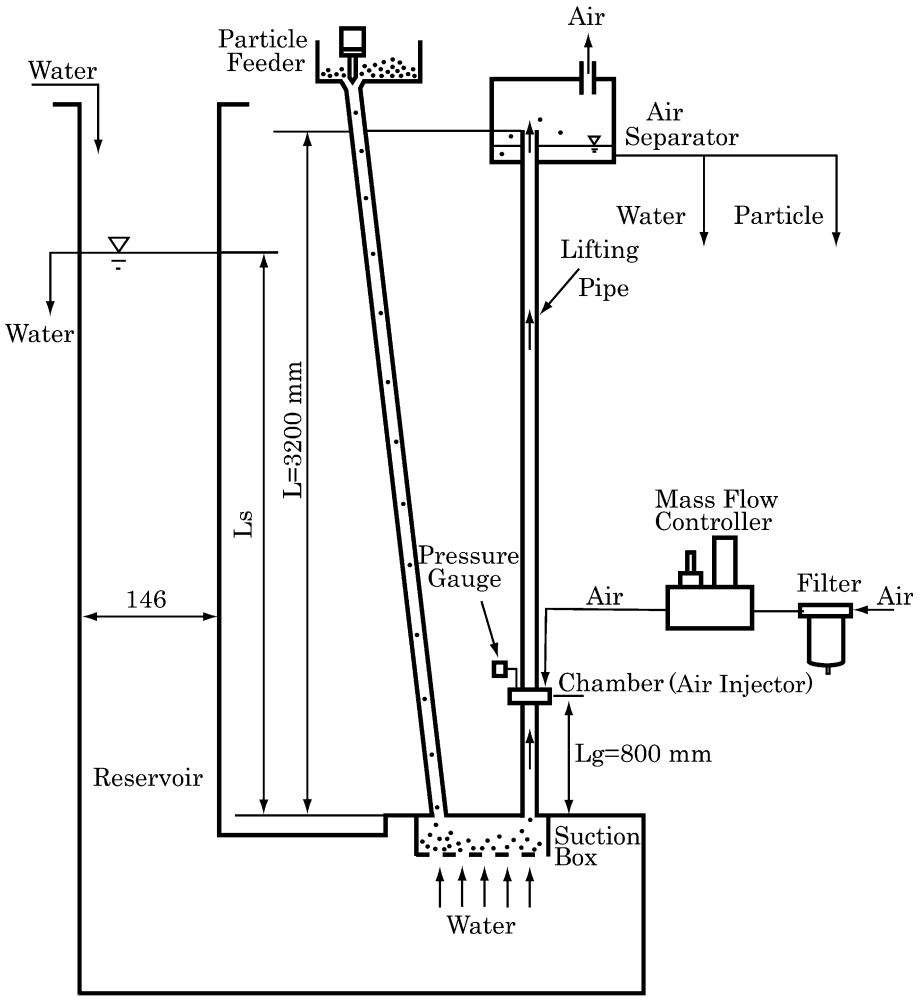

Fig. 3. Schematic of experimental setup.

The volume flow rate of the air is regulated and measured by a gas flow controller. In the present experiments, the gas volumetric flux (superficial velocity), j_{Ga}, reduced to the atmospheric pressure is in the range of $0\ \text{m/s} < j_{Ga} \leqslant 3.27\ \text{m/s}$. The measurement accuracy of j_{Ga} is within ± 0.03 m/s.

The volume flow rate of water, Q_L, is determined by the volume of discharged water and the sampling time, while the mass flow rate of solid particles, M_S, is measured by the discharged particle mass and the sampling time. Both Q_L and M_S are time-averaged values with sampling times of 30 or 40 s. The volumetric fluxes, j_S, for solid-phase and j_L, for liquid-phase are determined as follows:

$$j_S = \frac{M_S}{\rho_S A}, \quad j_L = \frac{Q_L}{A} \tag{2}$$

where A denotes the cross-sectional area of the lifting pipe. In addition, the measurement accuracy of j_L, and j_S are within ± 0.01 m/s, and ± 0.001 m/s, respectively.

The experiments are carried out under stable pump operating conditions: The mean flow rates of the injected air and solid particles are maintained at preset values, and the mean flow rate of discharged water is kept nearly constant. The measurement of water flow rate was carried out under a fixed experimental condition, at least, five times, and the arithmetic averaged data were obtained. The details of the experiments and the measurement method were explained and discussed in our prior study (Fujimoto et al. (2003)).

2.2. Video photography

The liquid–solid particles two-phase mixture flows along an upriser below the gas injector, while the gas–liquid–solid particles three-phase mixture flows above it. It was observed with naked eyes that the pump is operated at the slug or churn turbulent flow regime. Those flow patterns form a flow where liquid and gas bubbles alternately appear in the upriser above the gas injector. The flow in the pipe was unsteady and chaotic in nature. For understanding such unsteady flow in the pipe, photographic observation was performed, focused on the motion of particles. Successive video images at every 1/30 s were taken using a digital video camera with a resolution of 640×480 pixels. The camera was set horizontally and the exposure time was set to 1/210 s. Fluorescent lights (27 W and 15 W) were used as light source. The video images were transferred to a PC as digital data, and the trajectory of particles in the pipes was displayed on the PC.

Some experimental difficulties were encountered in the video photography. One was the distortion of images due to refraction of light at the interfaces, such as water/glass pipe wall, air/glass pipe wall, and air bubble/water interfaces. The cross section of the transparent pipe is circular and the air bubble/water interface is wavy. Thus, the light originated from the light source passes obliquely through such interfaces. Since the refractive indices of air, water, and glass are 1.0, 1.33, and 1.52 at wavelength 589.3 nm, respectively, refraction and reflection of light occur at the interfaces. If the incident angle of light to an interface is smaller than the critical angle determined by Snell's law, the light is partly reflected at the interface and partly passes through it. When the incident angle of light is equal or larger than the critical angle, total reflection occurs. Such complicated light path results in distortion of images. To minimize the effect of light refraction and/or reflection, the positions of light source were carefully chosen by trial and error method.

The time evolution of particle position was tracked using successive video images. In recoding the motion of particles in a pipe, particles painted red or yellow were prepared and a very small amount of colored particles were supplied together with normal (white) particles. It is noticed that no appreciable difference between the motion of the colored and normal particles was seen. In the video processing, such colored particles were picked up and were tracked. At relatively large particle fluxes, many particles are seen in a video frame. Colored particles often disappear in the video frame because they move behind other particles or away from the field of focus. Very few colored particles could be tracked in a relatively long period. In addition, it should be noticed that spatially exact tracks of particles cannot be followed because only one video camera was used and the light refraction occurs at every interface.

3. Results and discussion

3.1. Performance curves of an airlift pump in transporting liquid alone

Experiments without any particles were carried out before studying the flow of three-phase mixtures. The performance of the airlift pump is evaluated using the relation between the discharged liquid flux and the flux of injected air. For later convenience, the relation between the two fluxes is called performance curve. Fig. 4 depicts the performance curves of the present airlift pump for air–water two-phase flows. For all cases, S-shaped pipes are set above the gas injector. Every performance curve shows a well known trend reported in prior studies (for example, Yoshinaga and Sato, 1996; Fujimoto et al., 2003, 2004), namely, the volumetric flux of the discharged water increases with the volumetric flux of the injected air until reaching a peak, and then slightly decreases. Also, the discharged water flux is larger for larger submergence ratios associated with the difference between free water and discharge levels.

Appreciable reduction of pump performance occurs in the presence of local pipe bends. The straight pipe (pipe V) shows the best pump performance. The larger inclination angle of a pipe in the S-shaped portion gives rise to larger reduction of pump performance. One reason is the hydrodynamic head loss due to the pipe bends. Since the local curvature of the pipe bends is nearly the same (= 225 mm) for all S-shaped pipes, the head loss at the bends is larger for larger curving angles. In addition, the pipe length in the S-shaped portion is increased with the inclination angle, resulting in larger head loss due to wall friction. Consequently, the momentum losses are increased in the order of straight pipe, pipe (i), pipe (ii), and pipe (iii).

Fig. 5 shows the effect of the position of an S-shaped pipe (ii) on the pump performance. The S-shaped pipe (ii) is attached below the gas injector in the case of pipe C, while it is set above the injector in the case of pipe D. The discharged water flux in pipe C is slightly larger than that in pipe D. When the air–liquid two-phase mixture flows in the vertical airlift pump as shown in Fig. 1, it is observed with naked eyes that the flow pattern is slug flow (or churn-turbulent flow for larger gas fluxes). The liquid and the large air bubbles appear alternately along the pipe.

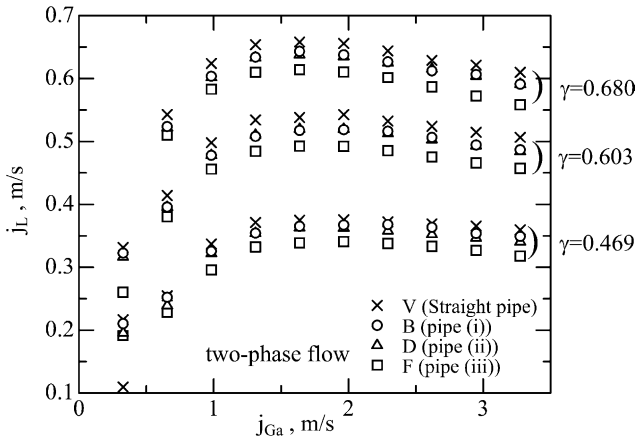

Fig. 4. Performance curves of an airlift pump for air–water two-phase mixtures.

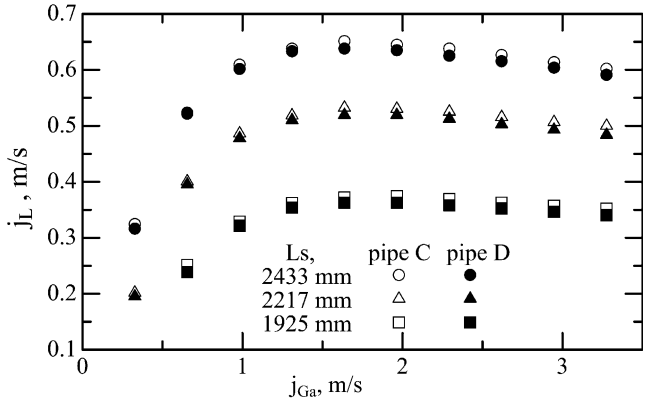

Fig. 5. Effect of the position of S-shaped pipe (ii) on pump performance.

The cross sectional diameter of bubbles is almost the same as the pipe diameter so that each air bubble pushes up the liquid. In the cases of inclined pipes, the shape of bubbles is not axisymmetric because of the effect of gravity. The air bubbles tend to flow in the upper part of the cross-section of the inclined pipe. The buoyancy force of air bubbles does not work effectively as a driving force. Therefore, a reduction of pump performance arises depending on the position of the S-shaped pipe.

From a view point of the flow pattern in the S-shaped portion, the results in Fig. 4 are discussed again. The reduction of pump performance in pipe (iii) is larger than that in pipe (i). One reason is the hydrodynamic head loss due to pipe bends, as previously explained. Another reason is because of the flow pattern. In pipe (iii), flow separation appears in the horizontal pipe region, as reported in our prior study (Fujimoto et al., 2004). The air flows in the upper cross-section of the pipe while the liquid exists in the lower section. In addition, the flow pattern changes from separated flow to slug or churn flow as the flow path shifts from the horizontal to the vertical region of the pipe. These phenomena cause a reduction of pump performance. On the other hand, the discharged water flux in pipe (i) is almost the same as that in the straight pipe V because of a smaller inclination angle of the S-shaped pipe. The momentum loss in the inclined portion is quite small.

3.2. Pump performance for three-phase flows

Performance curves were measured with supplying solid particles. Fig. 6(a) and (b) depict the performance curves of the airlift pump for (a) pipe D and (b) pipe C, respectively. In both figures, the discharged water flux is decreased by increasing the flux of solid particles, because the momentum is transferred from the liquid to the solid particles through the drag force. The performance curves show similar trends as in the cases with no particles: the volumetric flux of the discharged water increases with the volumetric flux of the injected air, reaches a peak, and then slightly decreases. An interesting feature is seen between the two performance curves for $j_S = 0.008$ m/s. The discharged water flux in pipe C is 0.45, 0.50, and 0.46 m/s for $j_{Ga} = 1.31$, 2.29, and 3.27 m/s, respectively, while the water flux in pipe D is 0.50, 0.52, and 0.49 m/s, respectively. As explained

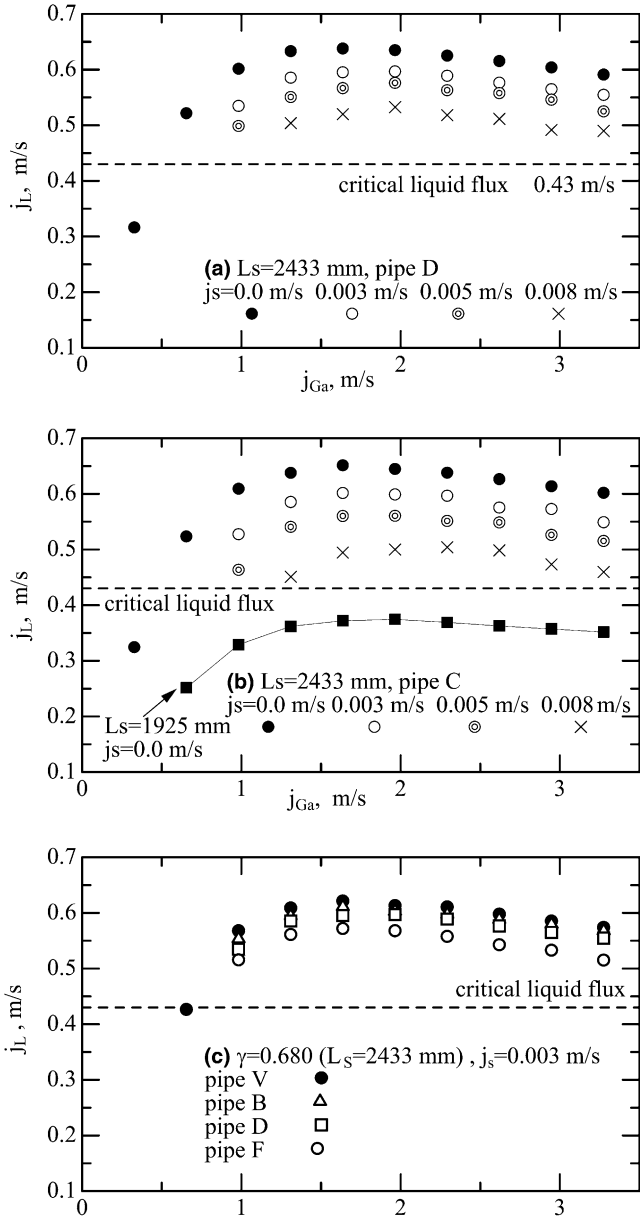

Fig. 6. Performance curves of an airlift pump for (a) pipe D and (b) pipe C, and (c) effect of the type of pipes on pump performance.

in the previous subsection, for cases of two-phase flows ($j_s = 0.0$ m/s), the discharged water flux in pipe C is slightly larger than that in pipe D. These results are opposite to the cases of two-phase flows ($j_S = 0.0$ m/s). The reason will be discussed later.

Fig. 6(c) represents the effect of the pipe type on performance curves for the submergence ratio, $\gamma = 0.680$, and volumetric flux of solid-phase, $j_S = 0.003$ m/s. Four types of the pipes, V (straight

pipe), B (pipe (i)), D (pipe (ii)), and F (pipe (iii)), are examined. With the S-shaped pipe attached above the gas injector in all cases, the air–liquid–solid particles three-phase mixtures flow in the S-shaped portion of the pipes. A large inclination angle in the S-shaped portion leads to a significant reduction of pump performance for the same reason as in the cases with no particles. The discharged water flux is increased in the order of pipe (iii), pipe (ii), pipe (i), and the straight pipe. In the case of $j_{Ga} = 0.65$ m/s, the preset volumetric flux of $j_S = 0.003$ m/s can be realized only by the straight pipe.

The dominant external forces acting on the dispersed solid particles in the liquid or air/liquid mixture are gravitational force and the drag force from the surrounding fluid. The drag force acts as the lifting force on the particle while gravity opposes it, when the particle mass density is higher than that of surrounding fluid. If the local surrounding fluid velocity is large enough, the particles are lifted along the pipe. Otherwise, only the surrounding fluid is transported. Thus, there is a critical boundary (critical velocity) at which the solid particles can be lifted. In our prior work, the critical boundary was investigated under various experimental conditions (Fujimoto et al., 2004). It was found that the critical value agrees reasonably well with the critical flux at which a single particle is kept at a certain point in a vertical pipe in a fully developed forced upward flow. The dotted lines in Fig. 6(a)–(c) represent the critical flux (= 0.43 m/s) for an alumina particle of 3 mm diameter obtained in our previous work. The particles are obviously lifted if the liquid flux is larger than the critical flux. Furthermore, it should be added that no particles are lifted in the case of $\gamma = 0.469$ where the water flux for two-phase flows never exceeds the critical flux (see Figs. 4 and 6(b)). It is also found that the pump performance for lifting solid particles is quite small and that almost all experiments were carried out under conditions close to the critical value. Such operating conditions should be avoided in actual use, though the critical flux is an important index when designing airlift pumps for transporting solid particles.

3.3. Photographic observations

3.3.1. Particle motion in pipe D

The flow characteristics in pipe D were observed using a digital video camera with the pipe (ii) attached above the gas injector. Fig. 7(a) displays instantaneous video images showing the flows below the gas injector for submergence ratio, $\gamma = 0.680$, volumetric flux for solid-phase, $j_S = 0.003$ m/s, and volumetric flux for gas-phase, $j_{Ga} = 1.96$ m/s. The liquid–solid particles two-phase mixture flows along a vertically straight pipe below the gas injector. The particles are dispersed randomly in the pipe. Since the airlift pump is operated in the slug or churn turbulent flow regime, the flow is essentially unsteady and flow pulsation occurs. As a consequence, the particle velocity changes temporally as well as spatially. Also, the local liquid velocity is small close to the pipe wall due to viscous shear stress, resulting in a radial velocity distribution. Particles move relatively fast near the axis, while particle velocity is small near the pipe wall.

For a better understanding of the particle motion, the time evolution of the particle position in a vertically straight pipe region was tracked using successive video images. Fig. 7(b) demonstrates examples of particle tracks under the same conditions in Fig. 7(a). The positions of the solid particles were directly measured from the video images. It is noted that the values in radial/horizontal coordinates are incorrect because only one camera was used and refraction of light occurs at the curved pipe wall, as previously described. The time interval of each successive two points is fixed

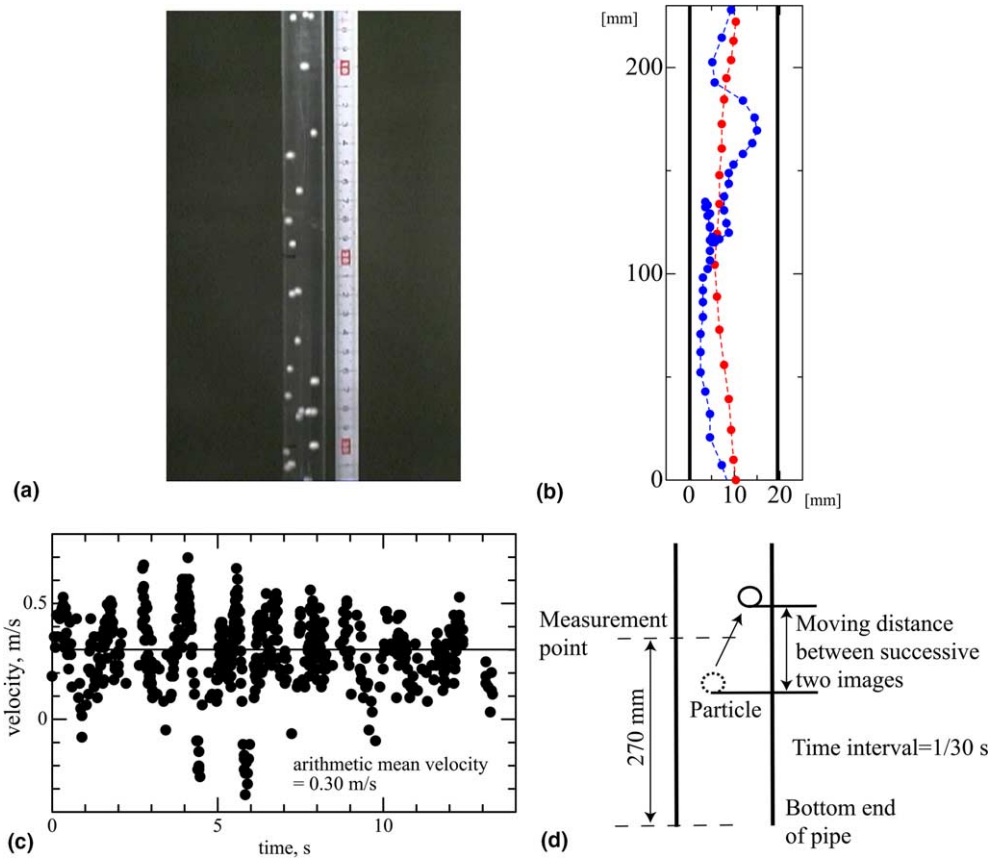

Fig. 7. (a) Instantaneous video images showing the flow below the gas injector, (b) examples of particle tracks in a pipe, (c) local upward velocity of particles passing through the vertical position of 270 mm above the bottom of the upriser, and (d) a schematic of measurement method. Note that the submergence ratio is $\gamma = 0.680$, volumetric flux for solid-phase is $j_S = 0.003$ m/s, and volumetric flux for gas-phase is $j_{Ga} = 1.96$ m/s.

to 1/30 s. Thus, the interval of each successive two points can be associated with the local particle velocity: the particle velocity is small in a small interval and vice versa.

It should be also noticed that two trajectories are plotted in the same figure, although they were videoscoped at different times. One particle moves up linearly near the axis of the pipe at a relatively large velocity. It has moved approximately 200 mm upward for a period of 0.5 s. The local velocity of surrounding liquid is considered to be relatively large and unvaried during this period.

The other particle shows very different motion. It ascends along the pipe, goes down, and moves up again. The particle velocity changes drastically. Such motion of the particle is due to the pulsation of flow and the radial profile of the liquid axial velocity with changes temporally as well as spatially. Since the velocity component of particles in the radial direction is non-zero, the particle occasionally hits the pipe wall, resulting in a sharp change of moving direction. A period of 1.3 s has been taken to move upward approximately 200 mm.

To investigate the unsteady motion of particles more quantitatively, local velocities of particles are measured. Fig. 7(c) represents the time evolution of local upward velocities of particles passing

through the vertical position of 270 mm above the bottom of the upriser under the same conditions in Fig. 7(a). The observation period is approximately 14 s and the number of data is 583. A schematic of measurement method is shown in Fig. 7(d). Every particle passing though the measurement line is picked up from successive two video images. The local upward velocity is determined by the time interval and corresponding moving vertical distance of particles. As the time interval between two successive video images is 1/30 s and is very accurate, the measurement error of the upward particle velocity is derived from the moving distance of particles. Its uncertainty is dependent on lens magnification. In the present case, the measurement accuracy of particle velocity is within ± 0.03 m/s. In addition, most particles passing through the measurement line could be identified during the observation period, because the local number density of particles is relatively small as shown in Fig. 7(a).

The negative velocity refers to the descending particle. As expected, the measured velocities are scattered. The particle motion is somewhat periodic due to the pulsation of the liquid flow. The particle velocity increases, it reaches a peak, decreases, and then increases again. This trend appears repeatedly. The maximum value of the particle velocity is approximately 0.7 m/s, which is larger than the discharged flux (superficial velocity) of liquid ($\sim$0.6 m/s). The minimum value is approximately -0.3 m/s. In addition, the solid line in the figure denotes the arithmetic mean value of measured velocities during the observation period ($= 0.3$ m/s).

The focus will now shift to the flow in the S-shaped portion attached just above the gas injector. Above the gas injector, the gas–liquid–solid particles three-phase mixture flows in the upriser. Fig. 8 shows the instantaneous images of three-phase mixtures in the S-shaped portion for $j_{Ga} = 0.98$ m/s. The video images are not very clear because of the presence of air bubbles. Reflection and refraction of light occurs at every liquid/solid interface. Thus, careful attention should be paid to understand the physics of the phenomena involved. After the gas injection, small air bubbles coalesce soon and relatively large air bubbles are formed. The volume fraction of liquid is

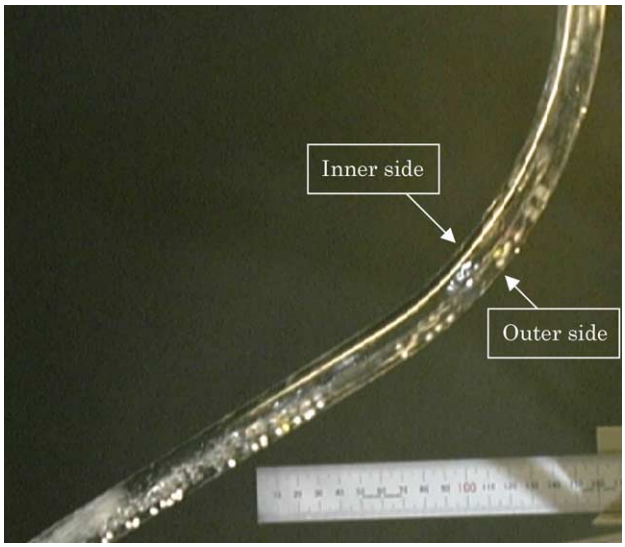

Fig. 8. Instantaneous image of three-phase mixtures in the S-shaped portion above the gas injector for $j_{Ga} = 0.98$ m/s.

sharply reduced, while local liquid velocity is increased. Air bubbles tend to flow in the upper area of the cross section due to buoyancy forces. Most particles are in the liquid and touch on the lower pipe wall due to gravity.

The time evolution of the particle position in the inclined pipe portion above the gas injector was tracked using successive video images. In doing so, very small amount of colored particles were supplied into the pipe together with normal particles. Fig. 9 displays examples of the tracks of colored solid particles for (a) $j_{Ga} = 1.96$ m/s and (b) $j_{Ga} = 0.98$ m/s, respectively. The time interval of each successive two points is 1/30 s. The black lines drawn in the figure indicate pipe walls. The particle velocity for $j_{Ga} = 1.96$ m/s is apparently larger than that for $j_{Ga} = 0.98$ m/s, suggesting that the local liquid velocity is larger.

The local velocity of particles varies with time, mainly due to the pulsation of the flow. The particle velocity is also dependent on the type of surrounding fluid. Since the density for gas-phase is appreciably smaller than that for the liquid-phase, the drag force exerted on particles in the air bubble is much smaller than that in the liquid. The gravity force is dominant in the air bubbles. In the region where the flow path shifts from the inclined to the vertical region of the pipe, particles are often trapped in the air bubbles and then slow down.

3.3.2. Particle motion in pipe C

Photographic observations are carried out in the case where pipe (ii) is attached below the gas injector. Fig. 10 shows photographs of the flow for the submergence ratio of $\gamma = 0.680$, a constant volumetric flux of solid-phase, $j_S = 0.003$ m/s, and the volumetric flux of gas-phase of (a)

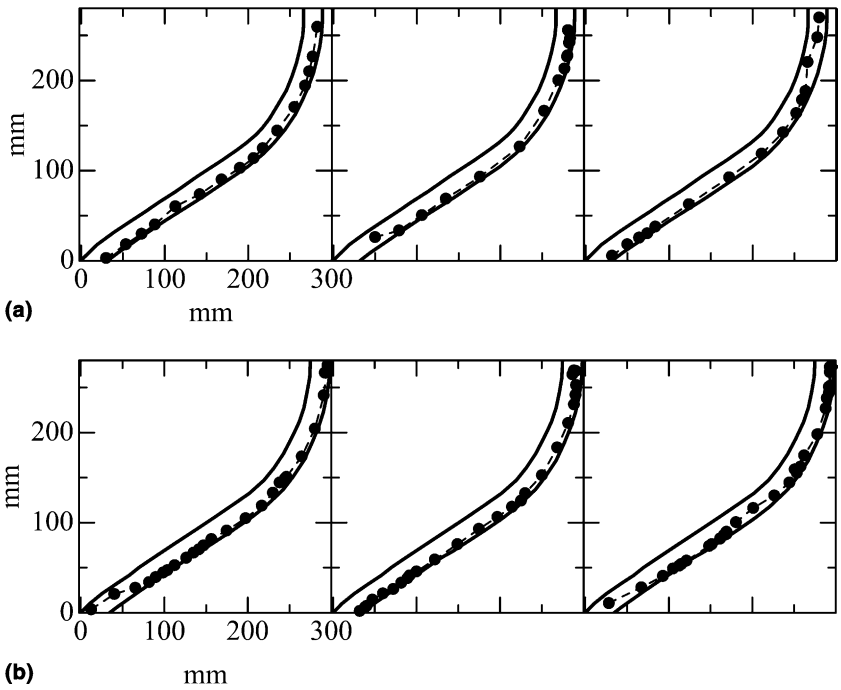

Fig. 9. Particle tracks in the S-shaped portion above the gas injector for (a) $j_{Ga} = 1.96$ m/s and (b) $j_{Ga} = 0.98$ m/s.

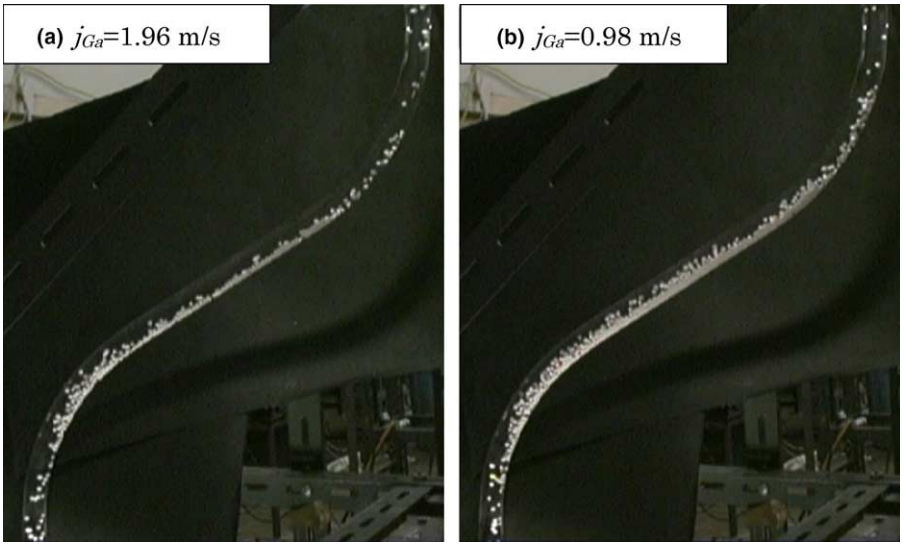

Fig. 10. Instantaneous images of three-phase mixtures in the S-shaped portion below the gas injector for $\gamma = 0.680$, $j_S = 0.003$ m/s, and (a) $j_{Ga} = 1.96$ m/s and (b) $j_{Ga} = 0.98$ m/s.

$j_{Ga} = 1.96$ m/s and (b) $j_{Ga} = 0.98$ m/s, respectively. The liquid–solid particles two-phase mixture flows in the S-shaped portion. The number of particles is obviously very large compared to the cases in Fig. 8. Many solid particles are seen at the lower pipe wall in the inclined pipe portion. A bed of particles is formed along the lower pipe wall in both cases. The number density of particles for $j_{Ga} = 0.98$ m/s is larger than that for $j_{Ga} = 1.96$ m/s. Since the volumetric flux of solid-phase is the same, this fact suggests that the local mean velocity of particles along the pipe is smaller.

In the particle bed, the effects of inter-collision of particles, gravity, and friction between moving particles and pipe wall are significant, while the drag force between liquid and particles is less effective. Accordingly, particles are almost stagnant or move very slowly downward along the inclined pipe wall. The flow area for the liquid-phase is obviously reduced due to the presence of stuck particles. Some particles flow in the upper cross-sectional area of the pipe at a relatively large velocity. The trajectory of such particles is non-straight for several reasons such as collision with the pipe wall, gravity and complex fluid motion. Thus, most of the particles are trapped in the particle bed and only a few reach the upper vertical pipe section. In addition, the formation of the particle bed in the inclined section is also observed in pipe (i). In the present work, almost all experiments are carried out under conditions close to the critical flux, as previously mentioned. The liquid velocity below the gas injector is relatively small. This may be the reason for the formation of the particle bed in the inclined section.

The performance curves for three-phase flows were reported in Section 3.2. It was found that the discharged water flux in pipe C is smaller than that in pipe D when the particle flux is relatively large. The reason is the presence of the bed of particles which is formed in the inclined portion against the gravity because of the momentum transfer from the liquid to the solid particles. The momentum transfer increases when the number of particles in the bed increases. In pipe C,

such momentum loss for the liquid-phase is quite large, resulting in reduction of discharged liquid flux.

Incidentally, in the present experiments, a stable pump operation is realized in the following manner: (i) the air begins to blow into the riser pipe without supplying any particles, (ii) the injected air flux is adjusted to a preset value so that stable pump operation for air–water two-phase flow is achieved, (iii) then, particles begin to be supplied, (iv) eventually, the discharged particle flux becomes the same as the supplied particle flux. The pump operation for air–water–solid particles becomes stable. The particle bed is formed in the inclined portion until stable operation.

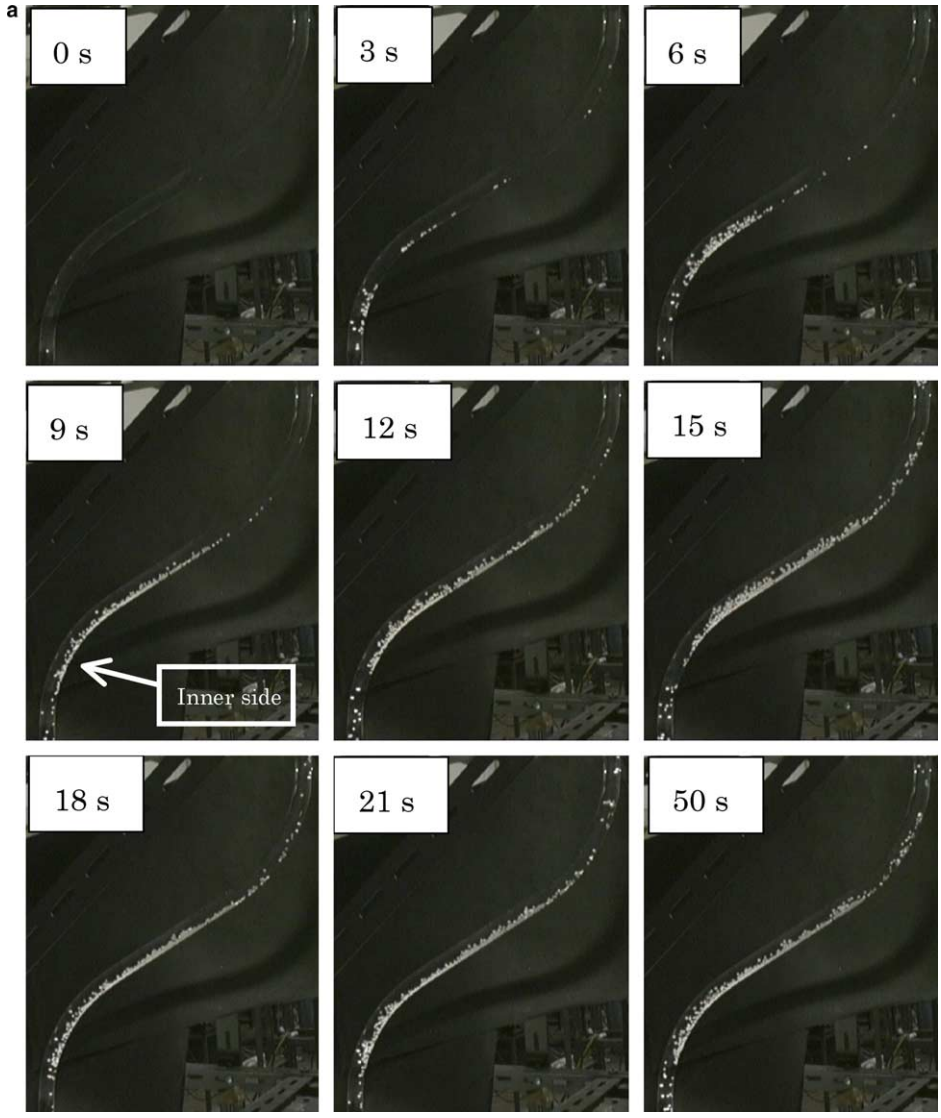

Fig. 11. Formation process of particle bed in the inclined pipe portion (a) $j_{Ga} = 1.96$ m/s and (b) $j_{Ga} = 0.98$ m/s.

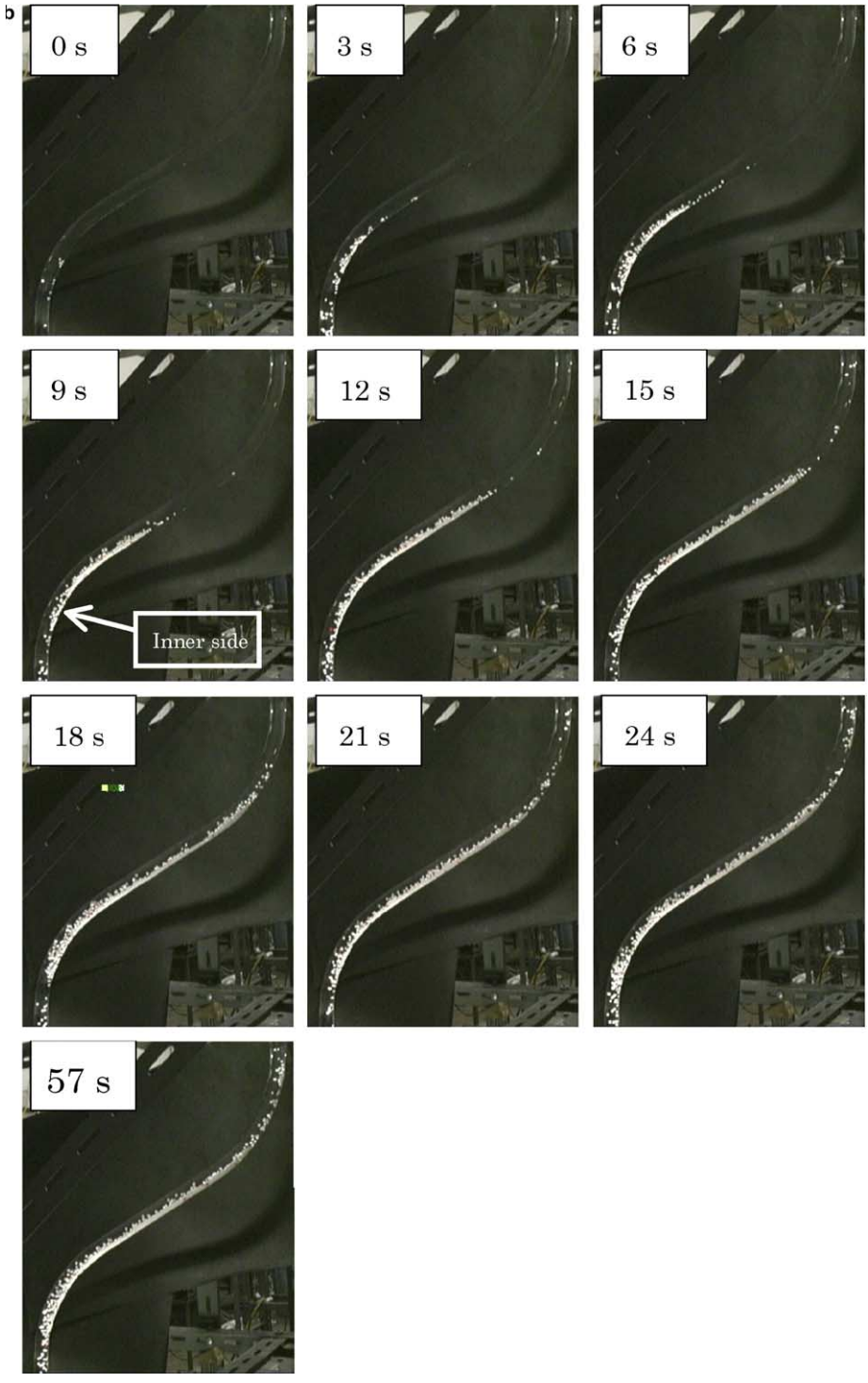

Fig. 11 (*continued*)

Fig. 11 depicts the formation process of the particle bed in the inclined pipe portion after particles begin to be supplied. The results for (a) $j_{Ga} = 1.96$ m/s and (b) $j_{Ga} = 0.98$ m/s are shown. It is found that a swarm of particles is first formed at the lower bend of the inclined pipe. It gradually advances upward along the lower pipe wall as time passes. As the superficial sectional area of the pipe is reduced in the region where the particle bed is formed, the liquid velocity locally increases. Particles are transported over the particle bed at a relatively large speed. After the particles reach the top/upper end of the particle bed, they slow down, move to the lower pipe wall and become a part of the particle bed. The particle bed is developed until its top reaches the upper bend. Eventually, a stable operating condition is realized.

The presence of the particle bed in the inclined portion is unwelcome in actual use for two reasons, namely, reduction of pump performance and the possibility of pipe clogging by particles. The particle bed also poses a difficult question in building a theoretical model capable of predicting the pump performance for three-phase flow. The momentum loss due to the particle bed should be counted into the model in some way. However, the evaluation of the momentum loss is quite difficult, because the formation of the particle bed depends on many factors, including injected gas flux, particle flux, size and material density, dimensions of the inclined pipe (angle and length of the inclined portion). Very few data are available and no theoretical models taking account of the problem have been proposed. This is a big challenge for future studies.

4. Conclusions

The pump performance of a small airlift system having local S-shaped bends was investigated experimentally. The results obtained in the present study are summarized below:

(1) The utilization of locally bent uprisers causes a reduction of pump performance, though it is inevitable in actual use. The larger inclined angle of S-shaped pipes gives rise to larger reduction of performance.
(2) The particle velocity changes temporally as well as spatially. The particle motion is very complex in nature because of several factors such as flow pulsation, radial distribution of the liquid axial velocity, gravity and pipe wall.
(3) A bed of particles is formed in the inclined pipe portion, when the S-shaped pipe is set below the gas injector. Reduction of pump performance occurs due to momentum transfer from the liquid to the particles in the bed. There is also the possibility of pipe clogging by particles. Such operating conditions should be avoided in actual use.

References

Fujimoto, H., Ogawa, S., Takuda, H., Hatta, N., 2003. Operation performance of a small air-lift pump for conveying solid particles. Trans. ASME J. Energy Res. Technol. 125, 17–25.

Fujimoto, H., Murakami, S., Omura, A., Takuda, H., 2004. Effect of local pipe bends on pump performance of a small air-lift system in transporting solid particles. Int. J. Heat Fluid Flow 25-6, 996–1005.

Hatta, N., Omodaka, M., Nakajima, F., Takatsu, T., Fujimoto, H., Takuda, H., 1999. Predictable model for characteristics of one-dimensional solid–gas–liquid three-phase mixtures flow along a vertical pipeline with an abrupt enlargement in diameter. Trans. ASME J. Fluids Eng. 121, 330–342.

Kato, H., Miyazawa, T., Tiyama, S., Iwasaki, T., 1975. A study of an air-lift pump for solid particles. Bull. JSME 18-117, 286–294.

Weber, M., Dedegil, M.Y., 1976. Transport of solids according to the air-lift principle. Proc. 4th Int. Conf. on the Hydraulic Transport of Solids in Pipes, Alberta, Canada, H1-1-23 and X93-94.

Yoshinaga, T., Sato, Y., 1996. Performance of an air-lift pump for conveying coarse particles. Int. J. Multiphase Flow 22, 223–238.